Observations of the Infrared Outgoing Spectrum of the Earth from Space: The Effects of Temporal and Spatial Sampling

H. E. BRINDLEY AND J. E. HARRIES

Space and Atmospheric Physics Group, Imperial College, London, United Kingdom

(Manuscript received 16 September 2002, in final form 10 April 2003)

ABSTRACT

A recent comparison between data taken by two different satellite instruments, the Interferometric Monitor of Greenhouse Gases (IMG) that flew in 1997 and the Infrared Interferometer Spectrometer (IRIS) that flew in 1970, showed evidence of a change in the clear-sky greenhouse radiative forcing due to the increase in greenhouse gas concentrations between those years. A possibly even more intriguing question is whether the data can be used to extract unambiguous information about the radiative feedback processes that accompany such a change of forcing, especially cloud feedback. This paper is an investigation of this question, with particular reference to the uncertainties introduced into the differences between IMG and IRIS spectra due to their different patterns of temporal and spatial sampling. This has been approached by modeling the sampling problem, using high-resolution proxy scenes of top-of-the-atmosphere 11-μm brightness temperature, T_{B11}, taken from International Satellite Cloud Climatology Project (ISCCP) data, sampled according to the characteristics of IRIS and IMG, respectively. The results suggest that while the sampling pattern of the IRIS instrument is sufficiently well distributed and dense to generate monthly regional mean brightness temperatures that are within 1.5 K of the true all-sky values, the IMG sampling is too sparse and yields results that differ from the true case by up to 6.0 K. Under cloud-free conditions the agreement with the true field for both instruments improves to within a few tenths of a kelvin. Comparisons with the observed IMG–IRIS difference spectra show that these uncertainties due to sampling presently limit the conclusions that can be drawn about climatically significant feedback processes. However, further analysis using the sampling characteristics of the Advanced Infrared Sounder (AIRS) instrument suggests that as climate change progresses, spectral measurements may be able to pick out significant changes due to processes such as cloud feedback.

1. Introduction

The detection and attribution of climate change is an important goal. A number of papers have been published that seek to use the long record of surface or near-surface temperature measurements for this purpose (e.g., Santer et al. 1995; Tett et al. 1999). Alternative parameters, such as the vertical temperature structure, sea level pressure, rainfall, and so on have also been investigated as suitable variables of climate change (e.g., Barnett and Schlessinger 1987; Santer et al. 1996). Other workers (Kiehl 1983; Charlock 1984; Goody et al. 1996; Slingo and Webb 1997; Harries et al. 1998) have presented a variety of studies of the information content of the earth's outgoing longwave emission spectrum. This is the flux of energy between about 3- and 100-μm wavelength (3300 and 100 cm^{-1}), which cools the earth to maintain energy balance with the incoming shortwave radiation from the sun, absorbed by the planet. The characteristics of this spectrum are described in a number of publications (e.g., Goody and Yung 1989).

In a recent paper, (Harries et al. 2001, hereafter H01), we presented the results of a study in which we carefully intercalibrated and compared IR spectra obtained from the *Nimbus-4* spacecraft in 1970, by the Infrared Interferometer Spectrometer (IRIS), with spectra from the Interferometric Monitor of Greenhouse Gases (IMG), flown in 1997 on the *Advanced Earth Observing Satellite 1* (*ADEOS-1*) spacecraft. This work showed that, over large regions of the earth, the clear-sky emission spectrum showed detailed changes, which agreed well with theoretical expectations based on the known changes of greenhouse gases such as CO_2, CH_4, O_3, and chlorofluorocarbons 11 and 12. In this way it has been experimentally confirmed for the first time that the greenhouse forcing of the earth has, indeed, been changed through the growth of greenhouse gases.

Climate change is much more than just a change in this greenhouse forcing. It also involves the response of the whole system, as represented in the radiation field by the radiation feedbacks due to a variety of causes. The most important atmospheric radiative feedback processes are due to water vapor and clouds (Houghton et

Corresponding author address: Dr. H. E. Brindley, Space and Atmospheric Physics Group, Imperial College, Blackett Laboratory, Prince Consort Road, London SW7 2BZ, United Kingdom.
E-mail: h.brindley@ic.ac.uk

al. 2001). Since completing our work on the clear-sky spectrum, we have studied the possibility that changes in the earth's outgoing spectrum may also contain information about changes in these feedback processes. It would be a major step forward in confirming our understanding of climate change if such changes in the dominant feedback processes could be observed.

However, a major difficulty in using the IR spectra measured from space for this purpose is sampling in both time and space. When sampling the cloud-free atmosphere, evidence indicates that the spatial variability beneath the satellite track may usually be regarded as small enough that spatial sampling differences between different instruments are not a significant source of uncertainty. Likewise, temporal variability, as long as major effects like the diurnal cycle are taken into account, need not introduce large uncertainties. However, when observing cloudy skies, we can expect larger uncertainties from sampling differences. This arises because of the high-contrast spatial structure, at all scales, which can exist in the cloud field and because of their transient nature. Under broken clouds the surface variability will also contribute to the problem with the precise location of the clouds, in addition to their properties, determining the observed brightness temperature.

In this and a companion paper (Brindley and Harries 2003, hereafter BH), we therefore present the results of studies that seek to make quantitative estimates of the uncertainty associated with the change in the all-sky spectral outgoing longwave radiation (OLR) derived from the IRIS and IMG measurements. In BH, we investigated the uncertainty arising from the differing instrumental spatial fields of view. In the present paper, we present the results of a study in which we examine the uncertainty caused by both spatial and temporal sampling differences between the two sensors. We find that, indeed, this uncertainty is significant compared with the change signal we might expect to observe today; but, given a steady development of global climate change, and also given the new generation of spectral sensors being launched into space, we believe that within about a decade, some signals of feedback processes may be detectable.

2. Observations and methodology

Both *Nimbus-4* and *ADEOS-1* were sun-synchronous satellites, and hence would be expected to sample each point on the earth once every 12 h at the same local time. Work by Salby and Callaghan (1997) and Engelen et al. (2000) has shown that such a sampling pattern can result in systematic biases in atmospheric parameters, even when these are averaged over the timescale of a month. In fact, for the IMG instrument in particular the observing pattern is even more irregular, since the operational schedule of the instrument resulted in measurements that are clustered over a period of a few days per month (Kobayashi 1999).

The approach we adopt to investigate quantitatively the uncertainty that derives from differences in sampling by the two different satellite sensors is as follows. Three-hourly, 0.5° latitude–longitude fields of International Satellite Cloud Climatology Project (ISCCP) 11-μm brightness temperatures (denoted by T_{B11}), and corresponding clear-sky brightness temperatures ($T_{B11\mathrm{clr}}$) were obtained (Rossow et al. 1996). These data were taken during two regional campaigns, namely the Tropical Ocean Global Atmosphere Coupled Ocean–Atmosphere Response Experiment (TOGA COARE) and the Fronts and Atlantic Storm Track Experiment (FASTEX). The former took place from November 1992 to February 1993, and was situated over the warm pool region with the aim of better understanding the ocean–atmospheric coupling within the study area and describing the interactions, which might extend its influence to other regions (Webster and Lukas 1992). The latter, primarily designed to improve forecasting of end-of-storm-track cyclogenesis (Joly et al. 1997), occurred during January and February 1997 over the North Atlantic Ocean. While being too coarse to resolve fast subpixel-scale processes (e.g., the development and passage of individual cloud cells), the temporal and spatial resolution of the data should be sufficient to track longer-lived systems and to provide a good representation of the diurnal cycle (Salby and Callaghan 1997). In the TOGA COARE case, 2 months of ISCCP data were extracted (December 1992 and January 1993) in order to obtain a feel for the month-to-month variability in the T_{B11} fields. Over the FASTEX region only data for February 1997 were available.

For each available month the true all-sky monthly mean value of ISCCP 11-μm brightness temperature was calculated, assuming perfect sampling, and denoted as $T^*_{B\mathrm{true}}$. In order to be consistent with the IMG and IRIS comparisons reported in H01, each available month of ISCCP data was sampled according to the IMG (IRIS) observing times and locations for April–June 1997 (1970), including only those observations taken over ocean. These subsets of the data were then averaged to produce $T^*_{B\mathrm{IMG}}$ and $T^*_{B\mathrm{IRIS}}$—the monthly mean all-sky values of brightness temperature that would have been obtained by each instrument. Thus, each of the 3 months of ISCCP data has one $T^*_{B\mathrm{true}}$, but three $T^*_{B\mathrm{IMG}}$, and three $T^*_{B\mathrm{IRIS}}$ corresponding to the three different sampling patterns (April, May, June). The same procedure was then applied to the $T_{B,11\mathrm{clr}}$ data to generate corresponding clear-sky quantities. In this case the true clear-sky monthly regional mean was denoted $T^*_{B\mathrm{clr,true}}$, with the values obtained using the IMG and IRIS sampling characteristics labeled $T^*_{B\mathrm{clr,IMG}}$ and $T^*_{B\mathrm{clr,IRIS}}$, respectively.

For clarity, the results for each campaign are discussed separately, with the findings for the TOGA COARE region presented in section 3, and for the FASTEX area in section 4. The actual observed IMG and IRIS difference spectra for both regions are introduced in section 5 in order to assess whether the signals present in the spectra

are sufficient to overcome the sampling bias defined by our simulations. In section 6 we discuss the abilities of the Advanced Infrared Sounder (AIRS) instrument to accurately capture the true atmospheric state given its sampling characteristics. Conclusions to be drawn from this study are then provided in section 7.

3. TOGA COARE results

a. All-sky conditions

Figure 1 illustrates the monthly mean all-sky T_{B11} fields for each 3-h time slot for December 1992 over the area 20°S–20°N and 120°–190°E. The area-averaged value for each time slot is also provided. The smallest values of T_{B11} are indicative of high, opaque cloud tops, and are located within the ascending branches of the intertropical convergence zone (ITCZ) and South Pacific convergence zone (SPCZ). Predominantly clear conditions, associated with subsidence, are characterized by the warmest brightness temperatures located north and south of the regions of ascent. The pattern appears to show little variability with time slot and the distributions are consistent with longer-term climatological patterns of cloud fraction and water vapor (e.g., Peixoto and Oort 1992; Wu et al. 1993). Indeed, closer inspection of the monthly mean diurnal range (Fig. 2a) indicates that generally the amplitude of the daily cycle in T_{B11} at a given location is of the order of 10 K or less. Exceptions to this rule occur within the ITCZ over Indonesia and Papua, New Guinea, and within the SPCZ, where the range increases to ~15–25 K. Within these regions the phase of the daily cycle is rather variable, the timing of maximum and minimum daily T_{B11} values changing with the day of the month. Figure 2b illustrates the variation seen at point 1 in Fig. 2a; the lack of coherence is typical of other locations showing a high diurnal range. Similar phase variability is seen over those areas with a small monthly mean diurnal range (Fig. 2c). For completeness, plots of the temporal standard deviation through December for each time slot are shown in Fig. 3. The largest standard deviations correspond to the areas of lowest T_{B11} identified in Fig. 1, indicating that cloud formation and advection is generally confined to regions of convergence, and that cloud amount and type at a given pixel within these regions can show substantial day-to-day variation. Similar results are seen for 3-hourly T_{B11} means and associated standard deviations for January 1993. Differences between the area-averaged monthly mean 11-μm brightness temperature and $T^*_{B\text{true}}$ are within $\pm$1.2 K for all time slots for both months.

Figure 4 indicates the location of all the available IRIS and IMG observations over the TOGA COARE region during April, May, and June of 1970 (IRIS) and 1997 (IMG). Measurements pertinent to each month are split according to whether the given satellite was in an ascending or descending node. In the IRIS case (Figs. 4a,b) it is clear that many more observations are available from the southward (local night) orbit than for the northward daytime orbit. This is partly due to quality control, but mainly to the fact that much of the original IRIS data was lost (Iacono and Clough 1996). The monthly IRIS orbits show a small temporal drift in the *Nimbus-4* equator crossing time of approximately 2 min over the 3 months. In the IMG case (Figs. 4c,d), the paucity of observations reflects the operational schedule of the instrument, with approximately 3 times as many observations available for April compared to any other month. There is a bias toward a greater number of local night observations except for May, where all the available measurements were taken during the day.

Table 1 provides the differences between the true regional monthly mean 11-μm brightness temperature values ($T^*_{B\text{true}}$) and those generated using IRIS ($T^*_{B\text{IRIS}}$) and IMG ($T^*_{B\text{IMG}}$) sampling patterns characteristic of April–June under all-sky conditions. The absolute values of $T^*_{B\text{true}}$ are also given in each case. Unsurprisingly, given the level of coverage, in general the IRIS sampling pattern does a much better job of estimating the mean, with an average difference between the true value of average brightness temperature and the simulated values of less than 1.5 K for the six cases considered. The results of the IMG simulation are rather different. Under the April sampling strategy, where IMG attains its best coverage, the agreement between simulated IMG means and the true values is of a similar level to IRIS, with discrepancies of less than 2 K. Consequently, the maximum absolute simulated differences between the two instruments for this month, $\Delta T_{B\max}$, are of a similar magnitude. However, for May and June, the poor IMG sampling (Fig. 4) results in large deviations from the true means. Values of $\Delta T_{B\max}$ in these cases can reach 6 K.

b. Clear-sky conditions

Statistics pertinent to the monthly mean brightness temperature fields for December 1992 are presented in Table 2 for clear-sky conditions. The area-averaged 11-μm brightness temperatures for each time slot show approximately one-fifth of the diurnal variability seen under all-sky conditions, with an associated reduction in the range of T_{B11} values observed at each interval. The distribution of these values is also relatively constant with time slot, although there is a clear daily cycle at most locations (not shown). As for the all-sky data, clear-sky values for January 1993 show a similar pattern of behavior.

Details of the deviations between the true and instrument-sampled regional monthly means for clear-sky conditions are presented in Table 3. The numbers of measurements making up the mean in each case are identical to the figures provided in Table 1. The uniformity of the clear-sky T_{B11} field is reflected in the small spread of the differences for both the IRIS and IMG values despite the discrepancy in the number of samples

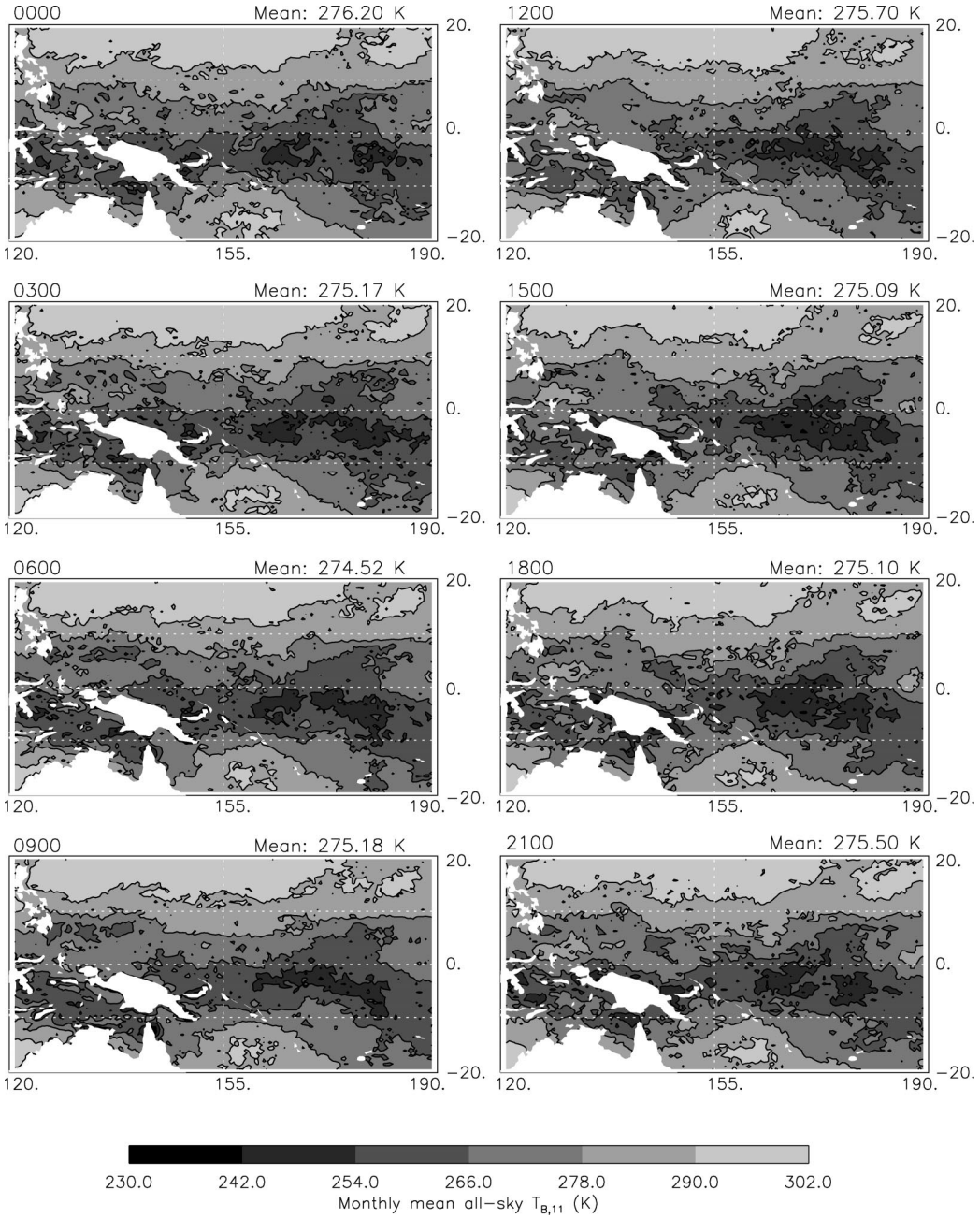

FIG. 1. Monthly mean all-sky T_{B11} fields for each 3-h time slot for Dec 1992 over the area 20°S–20°N and 120°–190°E. Values are derived from ISCCP DX data associated with the TOGA COARE experiment.

used to calculate the means. All the IRIS and IMG sampling patterns result in mean values that are within ± 0.3 K of the appropriate $T^*_{B\text{true}}$ value. Similarly, the values of $\Delta T_{B\text{max}}$ have a value of less than 0.5 K.

4. FASTEX results

a. All-sky conditions

Distributions of the monthly mean ISCCP T_{B11} for each 3-h slot over a portion of the FASTEX study area (30°–50°N, 315°–350°E) for February 1997 are provided in Fig. 5. Similar to the TOGA COARE results, the general pattern at each time is consistent, with the main feature being a southwest/northeast banding in the T_{B11} fields, values increasing systematically from the east coast of Greenland to the west coast of Portugal. This pattern is itself primarily a reflection of the surface temperature fields with the features of frontal cloud bands associated with typical midlatitude depressions superimposed. The distributions of the temporal standard de-

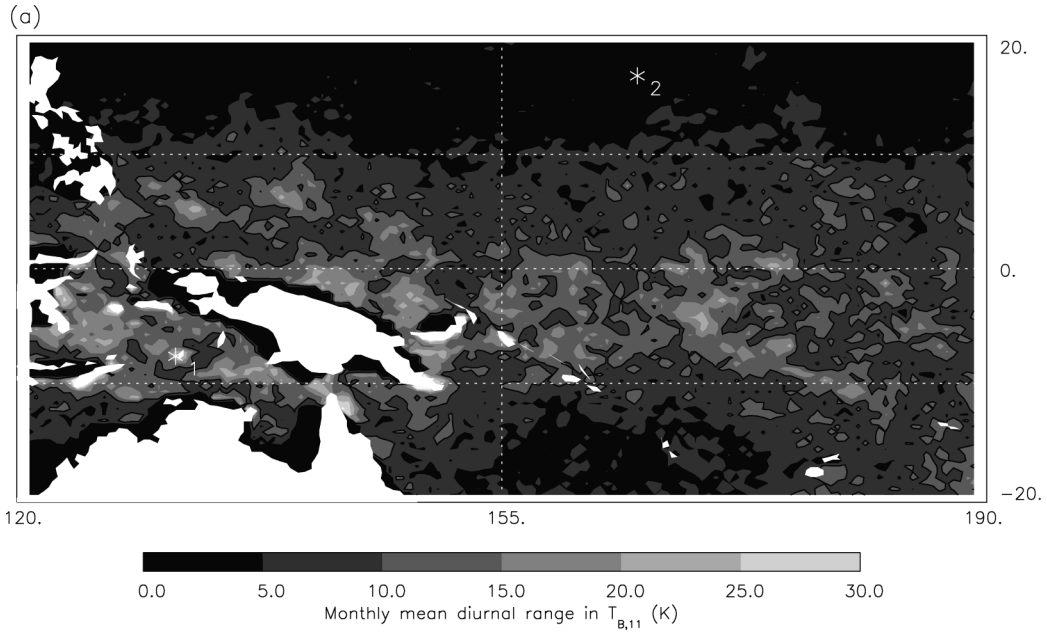

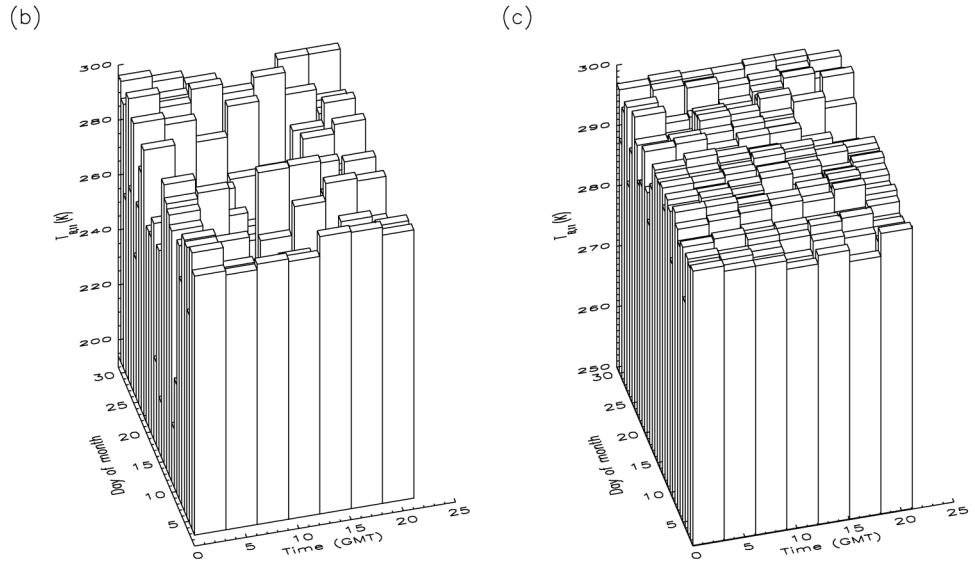

FIG. 2. (a) Monthly mean diurnal range in all-sky T_{B11} fields for Dec 1992 over the area illustrated in Fig. 1. (b) Progression of the diurnal distribution of all-sky T_{B11} values with day of month during Dec 1992 for point 1 (8.5°S, 130.0°E) in (a). (c) Same as (b) for point 2 (16.0°N, 164.5°E).

viations calculated for each time slot are also relatively constant with time of day, showing maximum values of between 15 and 20 K toward the northwestern corner of the region (not shown). Note that these values are of the order of half of the maxima seen in the TOGA COARE study zone.

Sampling tracks for IRIS and IMG across the FASTEX region for April–June are shown in Fig. 6. In contrast to the TOGA COARE case, for this region no IRIS measurements taken during local night are available. IMG observations are more equally distributed across both night and day for all months. Table 4 indicates the deviations between $T^*_{B\text{true}}$ and the monthly mean regional average brightness temperatures obtained for each instrument track. The absolute value of $T^*_{B\text{true}}$ in this case is 266.92 K. When all the available observations are included agreement both between the instruments and with the true mean is within ± 0.6 K for April. For the other two months the lack of IMG measurements in particular results in substantial deviations between T^*_{BIMG} and $T^*_{B\text{true}}$.

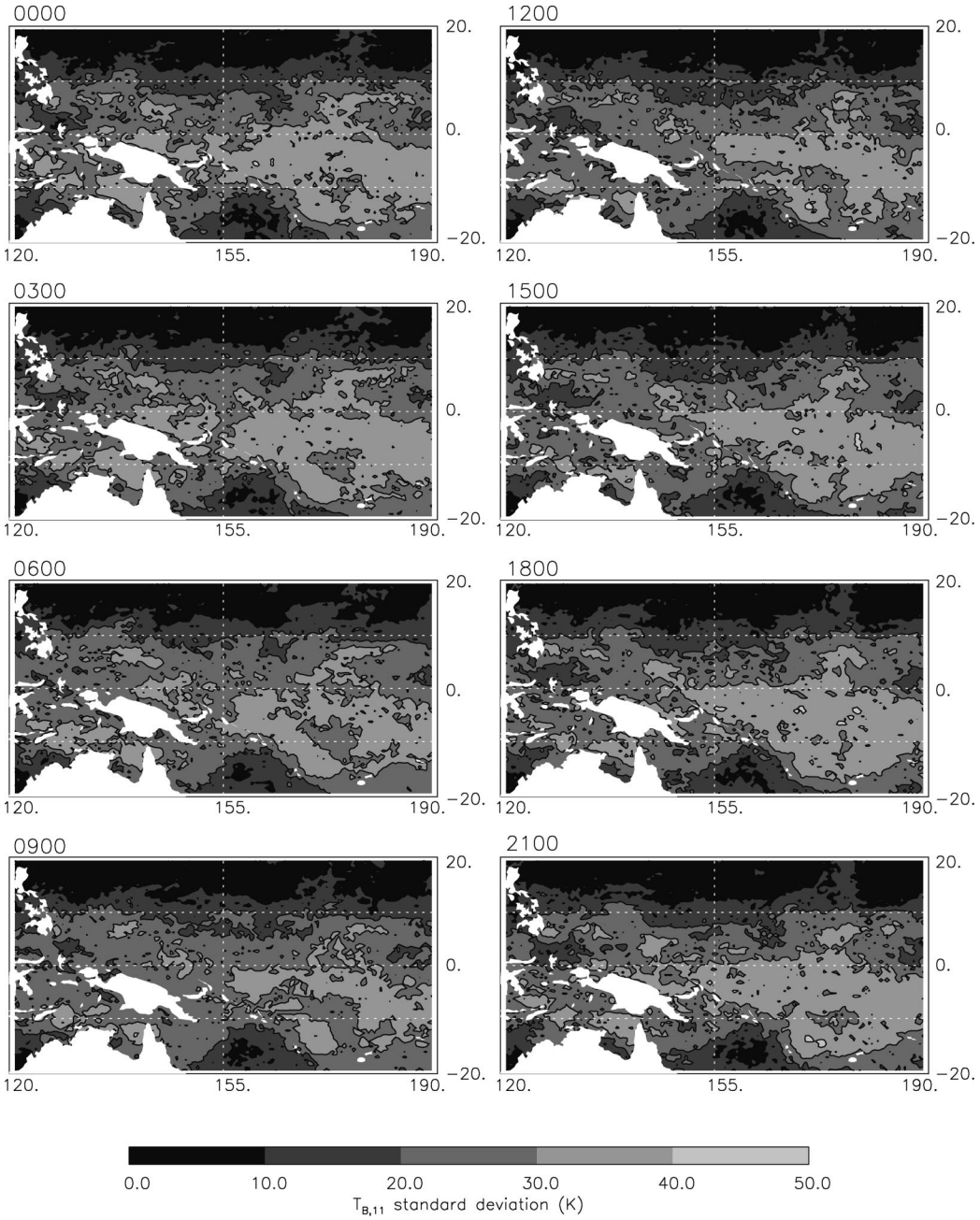

FIG. 3. Temporal standard deviation of the fields shown in Fig. 1.

A further question to be addressed concerns the impact of the uneven diurnal sampling of the IRIS instrument. Since the calculated T^*_{BIRIS} values are effectively daytime-only quantities, the IRIS sampling times were shifted forward by 12 h and an equivalent set of nighttime values, T^*_{BIRISN}, were obtained. A comparison of the two quantities (Table 4) shows no real consistent bias between daytime and nighttime values, with the sign of the difference dependent on the sampling pattern used.

b. Clear-sky conditions

Table 5 provides details of the clear-sky mean brightness temperature fields for each time slot relevant to the FASTEX area. As seen in the all-sky case, the diurnal variation in the mean fields is small compared with the spatial range of values at a given time, but does exhibit a coherent signal. To the northwest of the region values tend to be higher in the late afternoon/early evening, whereas in the southeast the brightness temperature

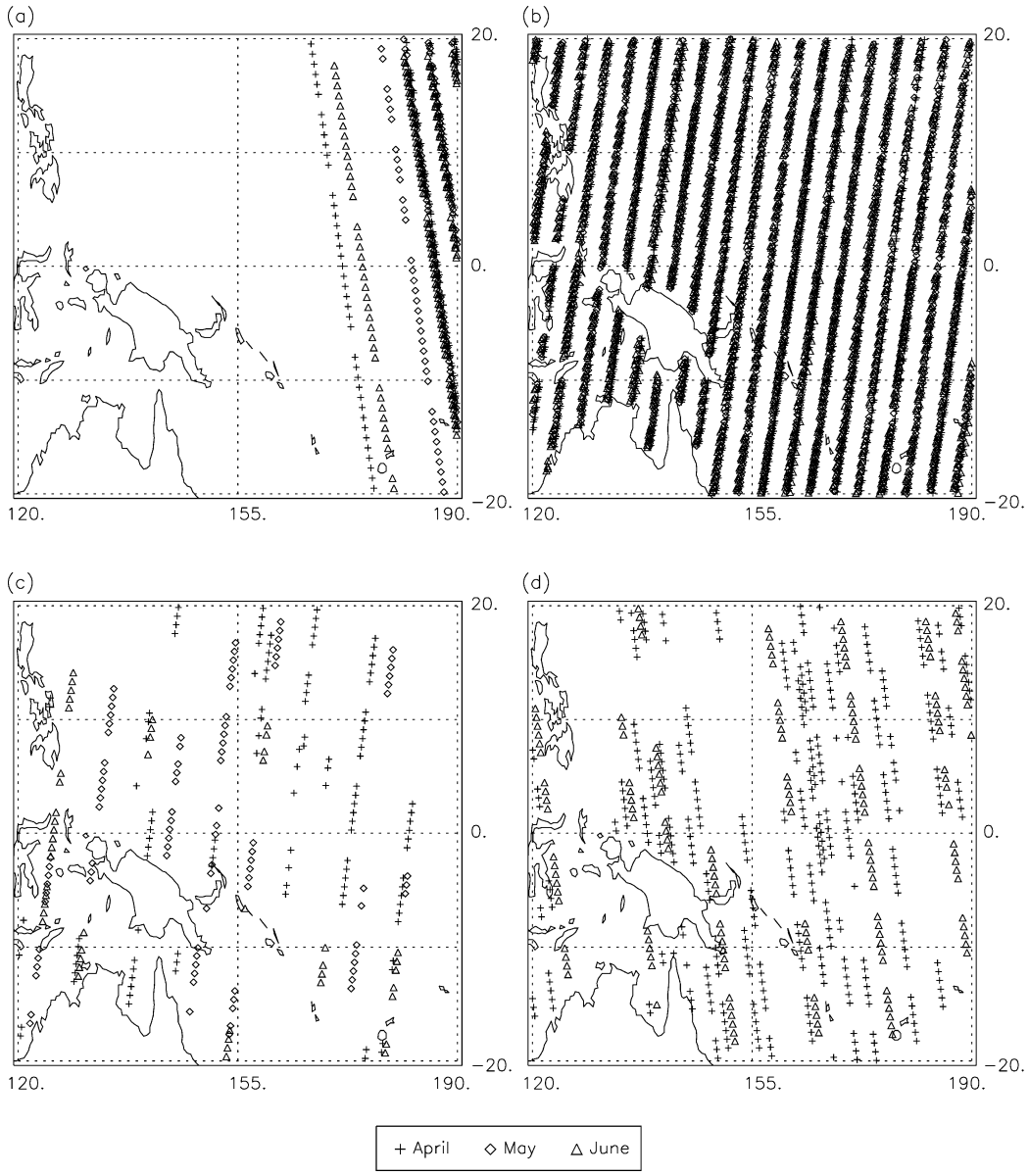

FIG. 4. Satellite sampling tracks over the TOGA COARE region for (a) IRIS northward node (1800–0600 UTC); (b) IRIS southward node (0600–1800 UTC); (c) IMG southward node (1800–0600 UTC); (d) IMG northward node (0600–1800 UTC).

TABLE 1. Differences (K) between the true regional mean 11-μm brightness temperature, $T^*_{B\text{true}}$, and the corresponding values obtained under IRIS ($T^*_{B\text{IRIS}}$) and IMG ($T^*_{B\text{IMG}}$) sampling patterns for all-sky conditions over the TOGA COARE measurement area. The number of samples for each month for each instrument is given by N_{IRIS} and N_{IMG}. Here, $\Delta T_{B\text{max}}$ is the maximum absolute difference in $T^*_{B\text{IMG}} - T^*_{B\text{IRIS}}$ that could occur due purely to sampling uncertainties.

Sampling pattern	N_{IRIS}	N_{IMG}	Dec 1992 $T^*_{B\text{true}} = 275.31$ K			Jan 1993 $T^*_{B\text{true}} = 277.26$		
			$T^*_{B\text{IRIS}} - T^*_{B\text{true}}$	$T^*_{B\text{IMG}} - T^*_{B\text{true}}$	$\Delta T_{B\text{MAX}}$	$T^*_{B\text{IRIS}} - T^*_{B\text{true}}$	$T^*_{B\text{IMG}} - T^*_{B\text{true}}$	$\Delta T_{B\text{MAX}}$
Apr	1345	544	−0.29	1.87	2.16	−1.49	0.70	2.19
May	1988	99	−0.13	4.88	5.01	0.25	2.78	3.03
Jun	1830	203	−0.50	−2.58	3.08	−0.71	5.28	5.99

TABLE 2. Area-averaged monthly mean 11-μm clear-sky brightness temperature over the TOGA COARE region for 3-hourly intervals during Dec 1992. The associated spatial std dev and range of each field is also provided.

Time (UTC)	Area-averaged monthly mean T_{B11clr} (K)	Std dev (K)	Range in monthly mean T_{B11clr} (K)
0000	295.78	1.59	18.68
0300	295.77	1.60	23.42
0600	295.77	1.72	27.65
0900	295.60	1.82	32.29
1200	295.55	1.77	20.53
1500	295.44	1.78	20.05
1800	295.54	1.77	20.99
2100	295.62	1.71	18.01

maximum occurs at around 1100 local time. The $T^*_{Bclr,true}$ value for the region is 283.56 K. Corresponding values for the IRIS and IMG sampling tracks during April–June are presented in Table 6. Similar to the TOGA COARE results, the level of agreement under clear-sky conditions is generally much improved, with both instruments obtaining regional monthly mean values that are within ± 0.8 K of the true value. Consequently the differences between the two instruments are of a similar magnitude.

5. Observed IMG–IRIS spectra

If the change in sampling between IRIS and IMG was not a major issue the values of ΔT_B calculated in the previous sections should always approach zero. Clearly, for several of the cases considered earlier this is not the case, and so it is of interest to investigate whether the observed IMG–IRIS brightness temperature differences exceed the levels of uncertainty quoted. Starting with the TOGA COARE region, the area average all-sky monthly mean brightness temperature (T_B) spectrum for each instrument for April is shown in Fig. 7a. IMG observations have been smoothed to match the spectral resolution of IRIS using the appropriate instrument function. The spectral range is limited to 710–1400 cm^{-1} because of the high noise levels of IMG at lower wavenumbers, and IRIS at upper values. Since the results quoted in the previous sections are based on 11-μm brightness temperatures, the normalized channel spectral response function is overplotted to provide an indication of its extent. Figure 7b indicates the spectral standard deviations associated with the mean spectra. There are two main reasons that could explain why the IMG standard deviations are higher than the corresponding IRIS values. First, even if both instruments had identical sampling patterns, the smaller field of view of IMG would mean that it would tend to ''see'' more extreme brightness temperatures than IRIS (see BH). Second, the different instrument sampling patterns may have resulted in IMG viewing a wider range of scenes relative to IRIS purely due to the timing and position of the formers' observations. Figure 7b also provides justification for using T_{B11} as an indicator of the error due to sampling considerations since for both instruments close to the maximum variability is seen in this region of the spectrum under all-sky conditions. Results for May and June show the same pattern of behavior.

IMG–IRIS monthly mean brightness temperature differences for April–June averaged over the TOGA COARE region are shown in Fig. 8. The horizontal dashed lines on each plot show the likely error range due to the sampling of the two instruments based on the calculations in section 3a. Looking first at the individual spectra, the signatures of gaseous absorption due to CH_4, O_3, and CO_2 noted by H01 in the clear-sky results are still apparent in all the traces. Note that under all-sky conditions one would expect to see smaller sampling errors associated with these regions than that provided by the T_{B11} estimate. All also exhibit a slight slope across the window region (800–1250 cm^{-1}), with differences tending to be more positive at the smaller wavenumbers. Across the window, the magnitude and sign of the differences seen vary greatly over the 3 months, but it is only in April that they can be said to emerge from the envelope of uncertainty associated with sampling. Even in this case, the differences are only of a larger magnitude than the error bounds at wavenumbers greater than 1080 cm^{-1}.

Figure 9 presents data analogous to Fig. 7 but for clear-sky conditions. The removal of cloudy spectra is achieved using the double-threshold method described in H01. Under clear conditions the pattern of variability is such that a sampling error based on the 11-μm channel can only really be considered representative of wavenumbers within the window region from 800–1250 cm^{-1}, excluding the 1040 cm^{-1} ozone band. At higher (lower) wavenumbers, variations in the distribution of water vapor (mid-upper-tropospheric temperature) play

TABLE 3. Same as for Table 1 for clear-sky conditions. In this case ΔT_{BMAX} is the maximum absolute difference in $T^*_{Bclr,IMG} - T^*_{Bclr,IRIS}$ that could occur due purely to sampling uncertainties.

Sampling pattern	Dec 1992 $T^*_{Btrue} = 295.63$ K			Jan 1993 $T^*_{Btrue} = 295.39$ K		
	$T^*_{Bclr,IRIS} - T^*_{Bclr,true}$	$T^*_{Bclr,IMG} - T^*_{Bclr,true}$	ΔT_{BMAX}	$T^*_{Bclr,IRIS} - T^*_{Bclr,true}$	$T^*_{Bclr,IMG} - T^*_{Bclr,true}$	ΔT_{BMAX}
Apr	−0.23	0.01	0.24	−0.15	−0.26	0.41
May	−0.17	0.11	0.28	−0.17	0.17	0.34
Jun	−0.25	−0.25	0.50	−0.25	−0.18	0.43

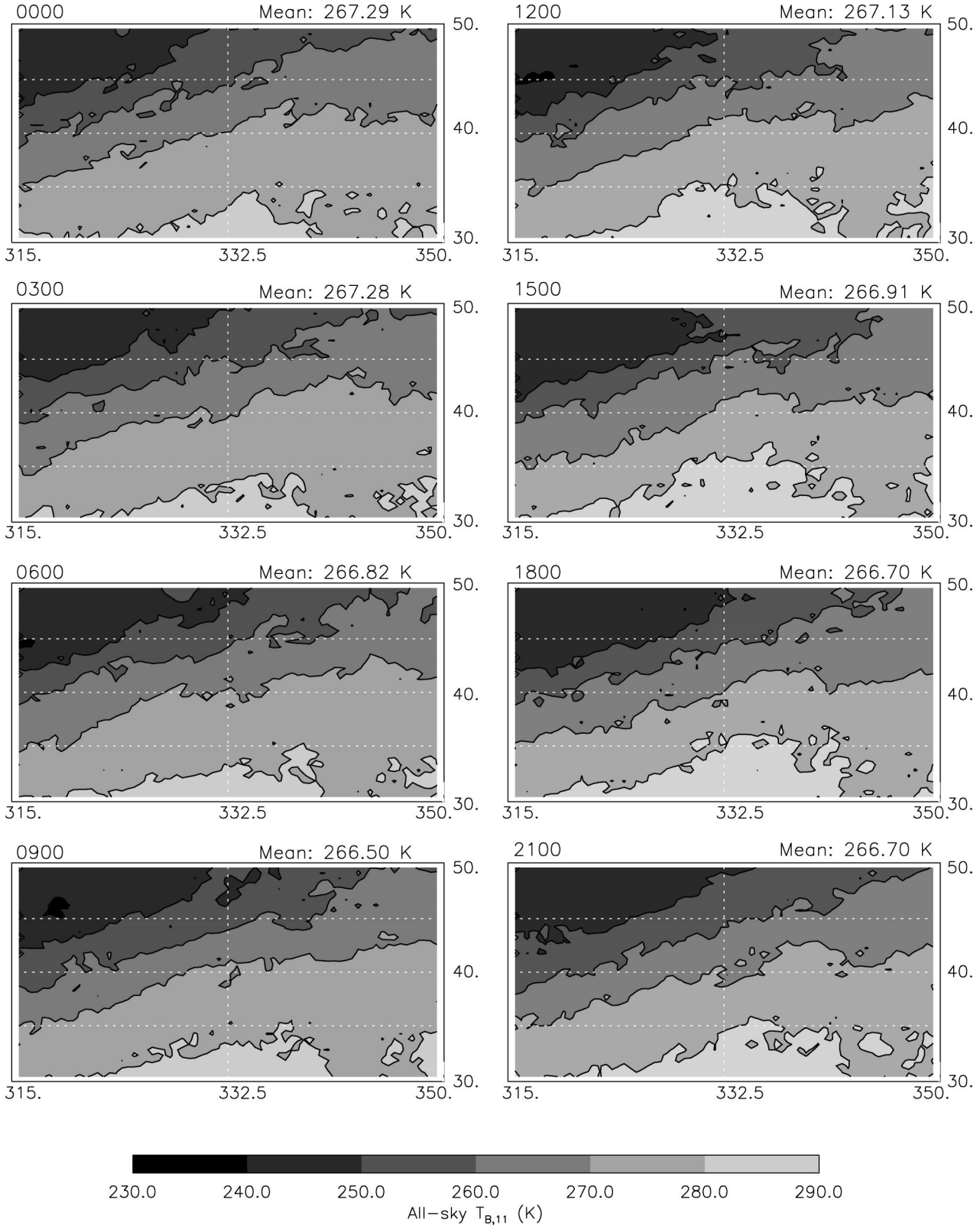

FIG. 5. Monthly mean all-sky T_{B11} fields for each 3-h time slot for Feb 1997 over the area 30°–50°N and 315°–350°E. Values are derived from ISCCP DX data associated with FASTEX.

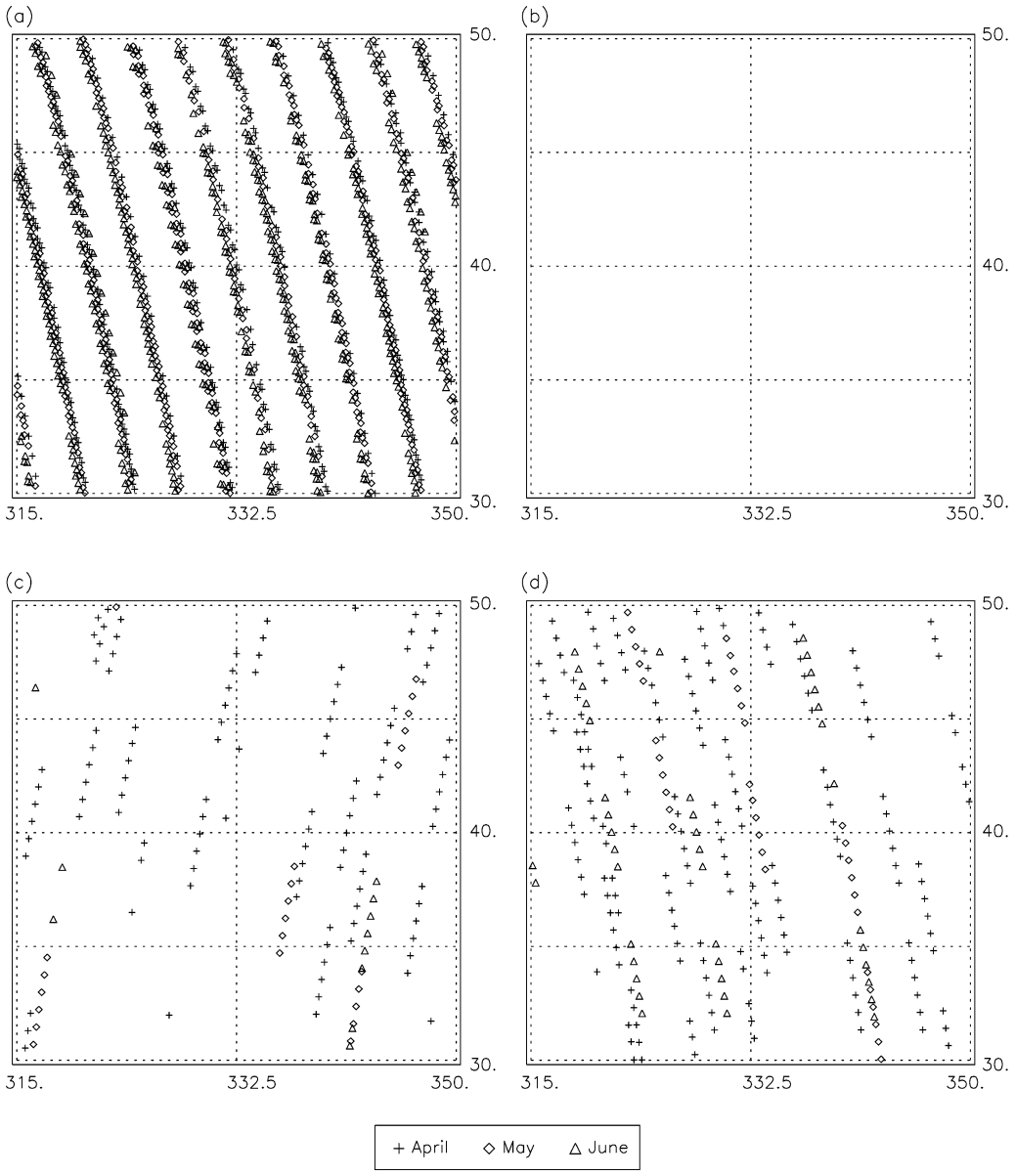

FIG. 6. Same as Fig. 4 for the FASTEX region.

the dominant role and a higher error would be appropriate (Fig. 9b). Monthly mean clear-sky difference spectra are shown in Fig. 10, along with the 11-μm error bound limited to the spectral region to which it applies. In all cases, at wavenumbers between 800 and 1000 cm^{-1} the window difference signal easily exceeds the error magnitude. In contrast, on the high-wavenumber side of the ozone band (1080–1250 cm^{-1}) the difference is systematically smaller, with values at, or just exceeding the error bounds. As noted in H01 some of this discrepancy could be due to the presence of residual cirrus cloud contamination in the nominally clear IRIS spectra.

TABLE 4. Same as Table 1 for the FASTEX measurement area.

Sampling pattern	N_{IRIS}	N_{IMG}	$T^*_{B\mathrm{IRIS}} - T^*_{B\mathrm{true}}$	$T^*_{B\mathrm{IRIS}} - T^*_{B\mathrm{IRISN}}$	$T^*_{B\mathrm{IMG}} - T^*_{B\mathrm{true}}$	$\Delta T_{B\mathrm{max}}$
Apr	308	297	−0.54	2.38	0.29	0.83
May	564	59	0.36	1.32	2.92	3.28
Jun	486	52	−1.42	−0.19	−2.48	1.61

Corresponding IMG–IRIS difference spectra for the FASTEX region under all- and clear-sky conditions are shown in Figs. 11 and 12, respectively. Again the appropriate error bounds are indicated on each plot. Similar to the TOGA COARE results, only the April all-sky differences exceed the sampling error (Fig. 11a), although in this case the magnitude of the observed

TABLE 5. Area-averaged monthly mean 11-μm clear-sky brightness temperature over the FASTEX region for 3-hourly intervals during Feb 1997. The associated spatial std dev and range of each field is also provided.

Time (UTC)	Area-averaged monthly mean T_{B11clr} (K)	Std dev (K)	Range in monthly mean T_{B11clr} (K)
0000	283.79	4.39	23.89
0300	283.53	4.15	21.56
0600	283.49	4.76	22.97
0900	283.18	4.92	23.94
1200	283.65	4.65	32.45
1500	283.59	4.63	43.54
1800	283.72	4.24	20.51
2100	283.54	4.38	23.11

change is substantially larger than the error estimate. This pattern is reversed under clear conditions, where April differences are within the calculated error bounds over the window region (Fig. 12a). For May and June the clear-sky changes over the same spectral range are larger in magnitude and are always above or just equal to the appropriate error estimates (Figs. 12b,c).

6. Sampling ability from AIRS

Clearly, one of the major barriers to extracting unambiguous information from an all-sky comparison of IRIS and IMG data is the limited sampling associated with, in particular, the latter instrument. Given the potential of spectrally resolved data to determine changes in, for example, vertical temperature structure, constituent concentrations, and cloud amount and properties, in this section the ability of the AIRS earth observation instrument to accurately capture the atmospheric state is investigated in the context of its sampling characteristics.

The AIRS instrument is a high-spectral-resolution grating spectrometer, measuring the earth's outgoing radiation in 2378 infrared channels (3.7–15.4 μm) at a spectral resolution ($\lambda/\Delta\lambda$) of 1200. A visible/near-infrared photometer also provides imaging capability in four channels from 0.4–1.0 μm. Mounted on the *Aqua* platform, AIRS views the ground through a cross-track rotary scan mirror that provides $\pm 49.5°$ ground coverage along with views to onboard spectral and radiometric calibration sources every 2.67-s scan cycle. The AIRS infrared spatial resolution is 13.5 km from the nominal orbit height of 705.3 km. Further instrument details can be found in Aumann and Pagano (1994). The

TABLE 6. Same as Table 3 for the FASTEX measurement area.

Sampling pattern	$T^*_{Bclr,IRIS} - T^*_{Bclr,true}$	$T^*_{Bclr,IMG} - T^*_{Bclr,true}$	ΔT_{Bmax}
Apr	0.15	−0.73	0.88
May	0.13	0.38	0.51
Jun	0.25	0.79	1.04

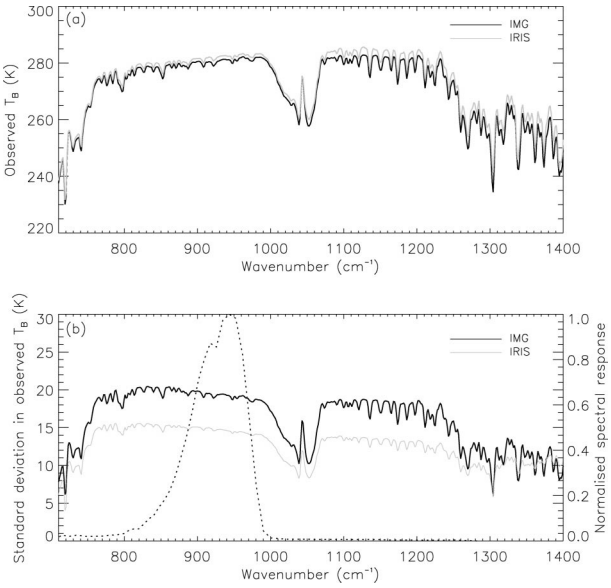

FIG. 7. (a) Apr mean observed IRIS and IMG all-sky T_B spectra over the TOGA COARE region for 1970 and 1997, respectively. (b) Std dev of the spectra in (a). The ISCCP 11-μm-channel filter function is given by the dotted trace.

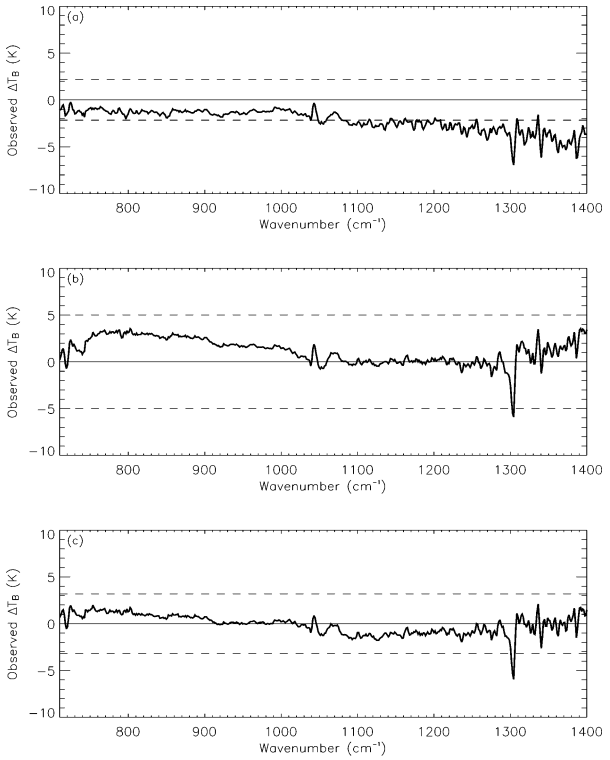

FIG. 8. IMG (1997)–IRIS (1970) all-sky T_B difference spectra for (a) Apr, (b) May, and (c) Jun over the TOGA COARE region. The dashed lines in each case provide an estimate of the likely error due to sampling taken from values of ΔT_{Bmax} in Table 1.

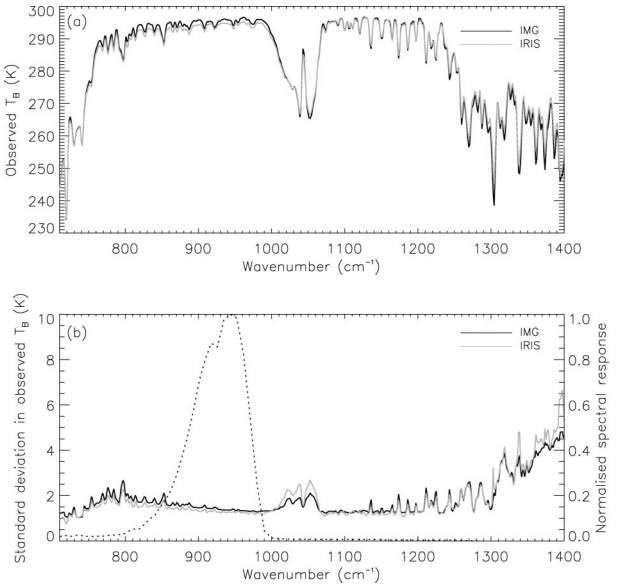

FIG. 9. Same as Fig. 7 for clear-sky T_B spectra.

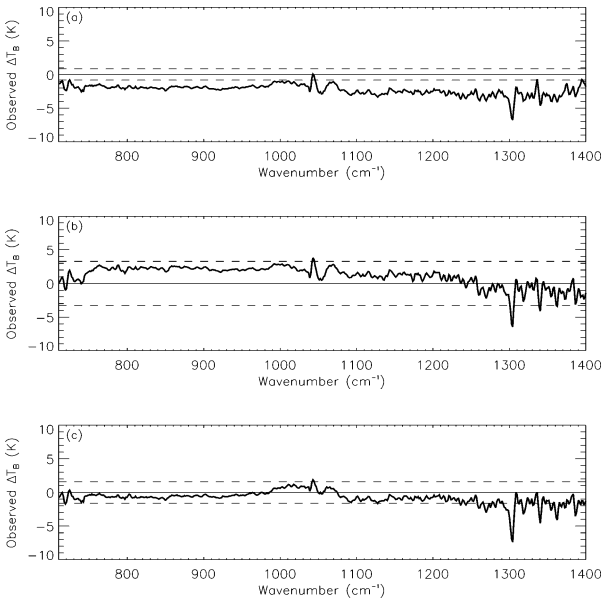

FIG. 11. Same as Fig. 8 for the FASTEX region. Error bounds are taken from Table 4.

Aqua orbit is polar sun synchronous, with an equator crossing time of 1330 in the ascending node and a 16-day repeat cycle.

Appropriate satellite tracks were calculated for April–June 2003 based on the *Aqua* orbital characteristics, and subsampled every 3 s to account for the AIRS scan cycle. These tracks were then used to sample the ISCCP data for both the TOGA COARE and FASTEX regions under all-sky (clear) conditions to obtain an estimate of the regional monthly mean 11-μm brightness temperature, $T^*_{B\mathrm{AIRS}}(T^*_{B\mathrm{clr,AIRS}})$. Table 7 provides details of the level of agreement between the true and AIRS-sampled values in each case. The agreement is of the order ± 0.5 K or better for all the scenarios considered, which is a notable improvement on the IRIS and IMG capabilities.

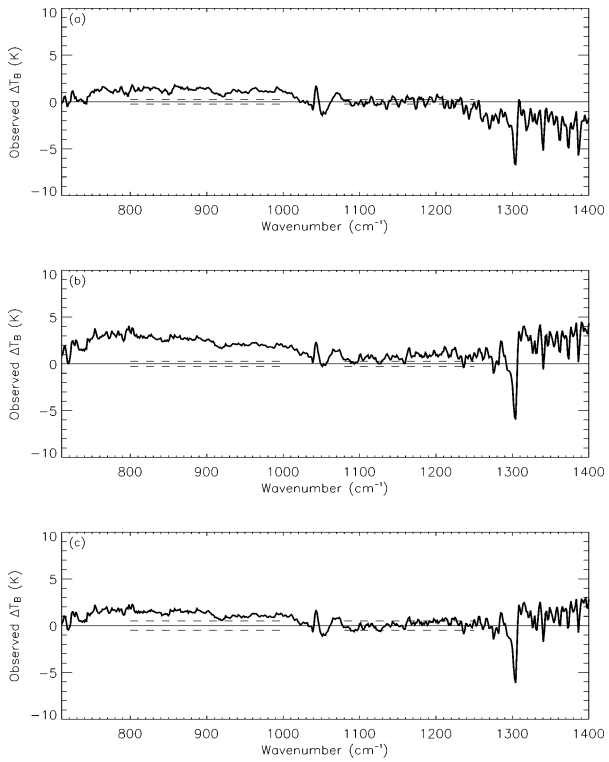

FIG. 10. Same as Fig. 8 for clear-sky T_B spectra. In this case error bounds are taken from Table 3.

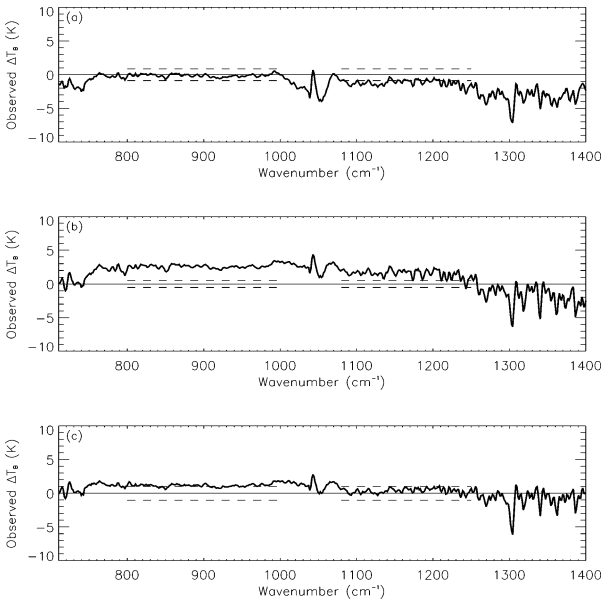

FIG. 12. Same as Fig. 9 for the FASTEX region. Error bounds are taken from Table 6.

TABLE 7. Differences (K) between the true regional mean 11-μm brightness temperature, $T^*_{B\text{true}}$, and the corresponding values obtained under AIRS (*Aqua*) sampling patterns for all-sky ($T^*_{B\text{AIRS}}$) and clear ($T^*_{B\text{clr,AIRS}}$) conditions over the TOGA COARE and FASTEX measurement areas. The number of samples for each month for each instrument is given by N_{AIRS}.

Sampling pattern	TOGA COARE					FASTEX		
	Dec 1992			Jan 1993		Feb 1997		
	N_{AIRS}	$T^*_{B\text{AIRS}} - T^*_{B\text{true}}$	$T^*_{B\text{clr,AIRS}} - T^*_{B\text{clr,true}}$	$T^*_{B\text{AIRS}} - T^*_{B\text{true}}$	$T^*_{B\text{clr,AIRS}} - T^*_{B\text{clr,true}}$	N_{AIRS}	$T^*_{B\text{AIRS}} - T^*_{B\text{true}}$	$T^*_{B\text{clr,AIRS}} - T^*_{B\text{clr,true}}$
Apr	32969	−0.18	−0.02	0.10	−0.03	8830	0.50	−0.13
May	33919	−0.22	−0.02	−0.18	−0.03	8815	0.53	−0.14
Jun	32903	−0.45	−0.01	−0.02	−0.05	8939	−0.20	−0.13

Indeed, under all but 3 of the 18 cases investigated, the differences between the true and AIRS-sampled values have a magnitude of less than 0.25 K.

7. Conclusions

The aim of this paper has been to provide some insight into the likely usefulness of IRIS and IMG observations in determining accurately any change in spectrally resolved brightness temperatures seen under clear- and all-sky conditions. The findings suggest that the sampling of IMG in particular is too coarse to provide an accurate representation of the atmospheric state. The exceptions to this general rule occur during April 1997, where the number of samples was increased threefold relative to the other months when observations were made, and under clear conditions in regions exhibiting low spatial and temporal variability in surface temperature.

For IRIS, temporal and spatial sampling is much more systematic and consistent. Over the regions considered, errors in the all-sky fields are a maximum of 1.5 K compared to values obtained given perfect sampling, the majority of these errors being less than 0.75 K. Assuming the signal magnitude remained unaltered, if similar accuracy were available from IMG the observed all-sky differences would exceed the uncertainty associated with sampling in most of the cases considered. Under clear conditions the true value is estimated to within tenths of a degree. The observed clear-sky IMG–IRIS window signal is such that it is only in the Tropics that it consistently exceeds the calculated sampling error. Whether this behavior is likely to be a result of ENSO-induced variability within the climate system will be investigated in a forthcoming publication.

While the IRIS and IMG observations provide a useful resource for analyzing the spectral forcing of the climate system due to enhanced levels of well-mixed greenhouse gases, a quantitative interpretation of the climatic response must be undertaken with some care. Besides issues concerning the limited length of the two datasets, it has been shown here that the sampling of both is only really sufficient to analyze clear-sky differences in terms of their being a true reflection of changes in the atmospheric state. A more all-encompassing comparison against IRIS may become possible with the availability of data from new spectrally resolved instruments such as AIRS. For the majority of regions and months considered here, our results suggest that if a difference between all-sky 11-μm monthly mean brightness temperatures measured by IRIS and AIRS was in excess of ~1 K it could be considered to be a true signature of change and not a sampling artifact. The question as to whether such a change could be considered to be representative of a climatic response to a given forcing, or was itself a natural fluctuation, would require further detailed analysis.

Acknowledgments. Thanks to three anonymous reviewers for their helpful comments. Helen Brindley is funded by the U.K. Meteorological Office under Agreement No. Met 1b/2861.

REFERENCES

Aumann, H. H., and R. J. Pagano, 1994: Atmospheric infrared sounder on the Earth observing system. *Opt. Eng.*, **33,** 776–784.

Barnett, T. P., and M. E. Schlesinger, 1987: Detecting changes in global climate induced by greenhouse gases. *J. Geophys. Res.*, **92,** 14 772–14 780.

Brindley, H., and J. Harries, 2003: The impact of instrument field of view on spectrally resolved brightness temperatures: Application to IRIS and IMG. *J. Quant. Spectrosc. Radiat. Transfer,* **78,** 341–352.

Charlock, T. P., 1984: CO_2 induced climatic change and spectral variations in the outgoing terrestrial infrared radiation. *Tellus,* **36B,** 139–148.

Engelen, R., L. Fowler, P. Glecker, and M. Wehner, 2000: Sampling strategies for the comparison of climate model calculated and satellite observed brightness temperatures. *J. Geophys. Res.*, **105,** 9393–9406.

Goody, R., and Y. L. Yung, 1989: *Atmospheric Radiation, Theoretical Basis.* 2d ed. Oxford University Press, 519 pp.

——, R. Haskins, W. Abdou, and L. Chen, 1996: Detection of climate forcing using emission spectra. *Earth Obs. Remote Sens.*, **5,** 22–33.

Harries, J., H. Brindley, and A. Geer, 1998: Climate variability and trends from operational satellite spectral data. *Geophys. Res. Lett.*, **25,** 3975–3978.

——, ——, P. Sagoo, and R. Bantges, 2001: Increases in greenhouse forcing inferred from the outgoing longwave spectra of the Earth in 1970 and 1997. *Nature,* **410,** 355–357.

Houghton, J. T., Y. Ding, D. J. Griggs, M. Noguer, P. J. van der Linden, and D. Xiaosu, Eds., 2001: *Climate Change 2001 The Scientific Basis.* Cambridge University Press, 944 pp.

Iacono, M., and S. Clough, 1996: Application of infrared interfer-

ometer spectrometer clear sky spectral radiance to investigations of climate variability. *J. Geophys. Res.,* **101,** 29 439–29 460.
Joly, A., and Coauthors, 1997: The Fronts and Atlantic Storm-Track Experiment (FASTEX): Scientific objectives and experimental design. *Bull. Amer. Meteor. Soc.,* **78,** 1917–1940.
Kiehl, J. T., 1983: Satellite detection of effects due to increased atmospheric carbon dioxide. *Science,* **222,** 504–506.
Kobayashi, H., 1999: Interferometric monitor for greenhouse gases. IMG Project Tech. Rep., IMG Mission Operation and Verification Committee, Central Research Institue of Electric Power Industry (CRIEPI), Komae Research Laboratory, Komae-shi, Tokyo, 45 pp.
Peixoto, J., and A. Oort, 1992: *Physics of Climate.* American Institute of Physics, 520 pp.
Rossow, W., and Coauthors, 1996: International Satellite Cloud Climatology Project (ISCCP): Documentation of new cloud datasets. World Meteorological Organization WMO/TD-No. 737, 115 pp.
Salby, M., and P. Callaghan, 1997: Sampling error in climate properties derived from satellite measurements: Consequences of undersampled diurnal variability. *J. Climate,* **10,** 18–36.
Santer, B., K. Taylor, T. Wigley, J. Penner, P. Jones, and U. Cubasch, 1995: Towards the detection and attribution of an anthropogenic effect on climate. *Climate Dyn.,* **12,** 77–100.
——, and Coauthors, 1996: A search for human influences on the thermal structure of the atmosphere. *Nature,* **382,** 39–46.
Slingo, A., and M. J. Webb, 1997: The spectral signature of global warming. *Quart. J. Roy. Meteor. Soc.,* **123,** 293–307.
Tett, S., P. Stott, M. Allen, W. Ingram, and J. Mitchell, 1999: Causes of twentieth century temperature change near the Earth's surface. *Nature,* **399,** 569–575.
Webster, P., and R. Lukas, 1992: TOGA COARE—The Coupled Ocean–Atmosphere Response Experiment. *Bull. Amer. Meteor. Soc.,* **73,** 1377–1416.
Wu, X., J. Bates, and S. Singh Kasala, 1993: A climatology of the water vapor band brightness temperatures from NOAA operational satellites. *J. Climate,* **6,** 1282–1300.